

International Journal of Nanoscience
 Vol. 21, No. 3 (2022) 2250035 (9 pages)
 © World Scientific Publishing Company
 DOI: 10.1142/S0219581X22500351



Synthesis of CuO NRs Using a Double Hydrothermal Method for a Highly Efficient Nonenzymatic Glucose Sensor

Haneen Ali Jasim*,‡ and Osama Abdul Azeez Dakhil†,‡

*Department of Physics, College of Science
 Mustansiriyah University, Baghdad, Iraq*

*haneenali@uomustansiriyah.edu.iq

†dr.osama@uomustansiriyah.edu.iq

Received 11 June 2022

Accepted 22 August 2022

Published

CuO NRs electrodes as nonenzymatic glucose sensors were successfully synthesized using a simple low-cost, high-benefit (double hydrothermal method) on indium tin oxide glass CuO/ITO with different concentrations. X-ray diffraction (XRD), field-emission scanning electron microscopy (FE-SEM), energy-dispersive X-ray spectroscopy (EDX), ultraviolet-visible spectroscopy, and investigations were used to confirm the nanostructures. XRD patterns of CuO explained all of the peaks may be attributed to CuO's monoclinic phase. FE-SEM presented nano rod-like shapes with a diameter range of 20–100 nm and was found to be uniformly and vertically grown on the ITO substrate. Besides, the energy gap of the CuO NRs was expanded to 3.3 eV, 3.1 eV and 3 eV, respectively. CuO NRs displayed the high activity of glucose sensing, with a sensitivity of (5805.7, 7365.7 and 994.8) $\mu\text{A Mm}^{-1} \text{cm}^{-2}$ with LOD (0.44, 0.4 and 0.35) μA , respectively. These results indicate that the sensor has a lot of potential for becoming a high-performance nonenzymatic glucose sensor with a simple, low-cost, and unique sensor design.

Keywords: CuO NRs; double hydrothermal method; glucose bio-sensor.

1. Introduction

The diagnosis of diabetes mellitus as a “chronic and metabolic disease” is based on the blood glucose level. Numerous health issues, including chronic kidney failure, stroke, cardiovascular disease, retinal damage to the eyes, and foot ulcers are caused by high blood sugar levels, or “glucose”.^{1,2} Therefore, early identification is essential to stop and avoid the life threatening complications brought on by high glucose levels. Recently, a variety of techniques have been used to monitor glucose concentration,

including electrochemical, colorimetric, piezoelectric, and thermoelectric based biosensors.^{3–9} Because of its unique characteristics of high sensitivity, superior selectivity, and ease of operation, the electrochemical approach is a promising tool for the manufacture of simple and low-cost glucose biosensors because of its unique characteristics of high sensitivity, good selectivity, and ease of operation.^{10,11} Traditional glucose biosensors based on glucose oxidase (GOx) are widely known for their great sensitivity and selectivity for glucose detection.

‡Corresponding author.

H. A. Jasim & O. A. A. Dakhil

Increased surface area, catalyzing the reaction, allowing the reaction to take place at low potentials,^{12,13} improved biomolecule adsorption,^{14,15} and facilitating the rapid transfer of electrons from the active center of the reaction to the electrode surface are all advantages of using nanomaterials in bio-sensor structures today. These approaches, however, have some major limitations, including difficult and multi-step immobilization procedures, heat and chemical instability, and a high cost, all of which limit their use.^{16–18} To overcome these challenges, nonenzymatic glucose biosensors based on noble metals (such as Pt, Pd and Au) have been successfully developed. Unfortunately, the expensive cost of the electrode materials prevents them from being widely used commercially.^{19,20}

CuO, NiO, Co₃O₄, Mn₃O₄, and other low-cost transition metal oxides have recently attracted a lot of attention as nonenzymatic glucose biosensors.^{21–24} Because of its strong electrochemical activity, adequate surface charge, and easily programmable surface structure, CuO, a *p*-type metal oxide semiconductor with a narrow band gap (1.2–1.9 eV), has been intensively explored for nonenzymatic glucose biosensing.

Several CuO-based materials-based nonenzymatic glucose biosensors have been successfully manufactured up to now. Nonenzymatic glucose biosensors have been made using CuO-based materials with various morphologies or topologies, such as nanoparticles,²⁵ nanorods,²⁶ and nanotube arrays.²⁷ In this study, we used a new simple double-hydrothermal method to manufacture CuO NRs with different concentrations, which was inspired by past research papers for the detection of an enzyme-free glucose sensor. The created sensor displayed excellent long-term stability and high sensitivity with low detection limits when it came to detecting glucose.

2. Experimental

2.1. Materials

Copper nitrate hydrate (Cu(NO₃)₂ · 5H₂O, purity 99.9%) was acquired from Scharlau, Spain, while hexamethylenetetramine (HMT, C₆H₁₂N₄, quality 99%) was obtained from Hi-media India. The indium tin oxide glass was supplied by Yingke Optical Products, Co. Ltd. in China (ITO). KOH with a purity of 99.5% was acquired from Scharlau, Spain. Absolute ethanol (C₂H₅OH) and distilled water

were utilized as specified. For electrochemical measurements, a glucose (Sigma Aldrich, 99.99% purity) solution with specific concentrations (0.5, 1 and 2) mM was produced.

2.2. Synthesis of CuO NRs by a double-hydrothermal method

To remove impurities from the surface of the Indium Tin Oxide glass (ITO) substrates (1.2 × 1.2 cm), they were washed in an ultrasonic bath with ethanol and distilled water for 15 min before being dried in an air stream. This approach consisted of two steps. To begin, dissolve 0.02 M (0.3 g) copper nitrate hydrate (Cu(NO₃)₂ · 5H₂O and 0.06 M (0.224 g) HMT in 80 ml DW for 15 min, or until the pH reaches 5. Inside the autoclave at 90°C, the ITO substrate was immersed in the aforementioned solution. After 4 h, the CuO film was washed with DW and dried on a hotplate for 15 min at 50°C. Second, under similar growth conditions, the CuO layer was immersed in a solution of Cu(NO₃)₂ · 5 H₂O (0.06 M) and HMT (0.06 M), and then thermally treated at 400°C for 2 h to improve the CuO film's crystal quality. This synthesis was carried out using a two-step hydrothermal method. The same previous steps are repeated to prepare different concentrations of 0.04 and 0.06 of CuO (Fig. 1).

2.3. Characterization

To characterize the films that were produced, a variety of methods were used. X-ray diffraction (XRD) and field-emission scanning electron microscopy were used to investigate the structural characteristics (FE-SEM). A PIXcel diffractometer equipped with a monochromatic CuK α X-ray source was used to perform $\theta/2\theta$ scans with a Bragg range of 20°–80°. The morphology of the formations was imaged using a Zeiss SIGMA VP-FESEM. A Double Beam Li-2800 spectrophotometer was used to detect absorption across a wavelength range of 200–900 nm.

2.4. Glucose biosensor measurements

To conduct electrochemical measurements, a Keithley 2430-C Source Meter (SMU) Instrument with contact check/GPIB interface and 1kW pulse mode was employed (A Tektronix Company). As shown in Fig. 2, all electrochemical measurements were performed with a three-electrode setup

1	53
2	54
3	55
4	56
5	57
6	58
7	59
8	60
9	61
10	62
11	63
12	64
13	65
14	66
15	67
16	68
17	69
18	70
19	71
20	72
21	73
22	74
23	75
24	76
25	77
26	78
27	79
28	80
29	81
30	82
31	83
32	84
33	85
34	86
35	87
36	88
37	89
38	90
39	91
40	92
41	93
42	94
43	95
44	96
45	97
46	98
47	99
48	100
49	101
50	102
51	103
52	104

AQ: Pls approve
short title.
ok, approved

Synthesis of CuO NRs Using a Double Hydrothermal Method

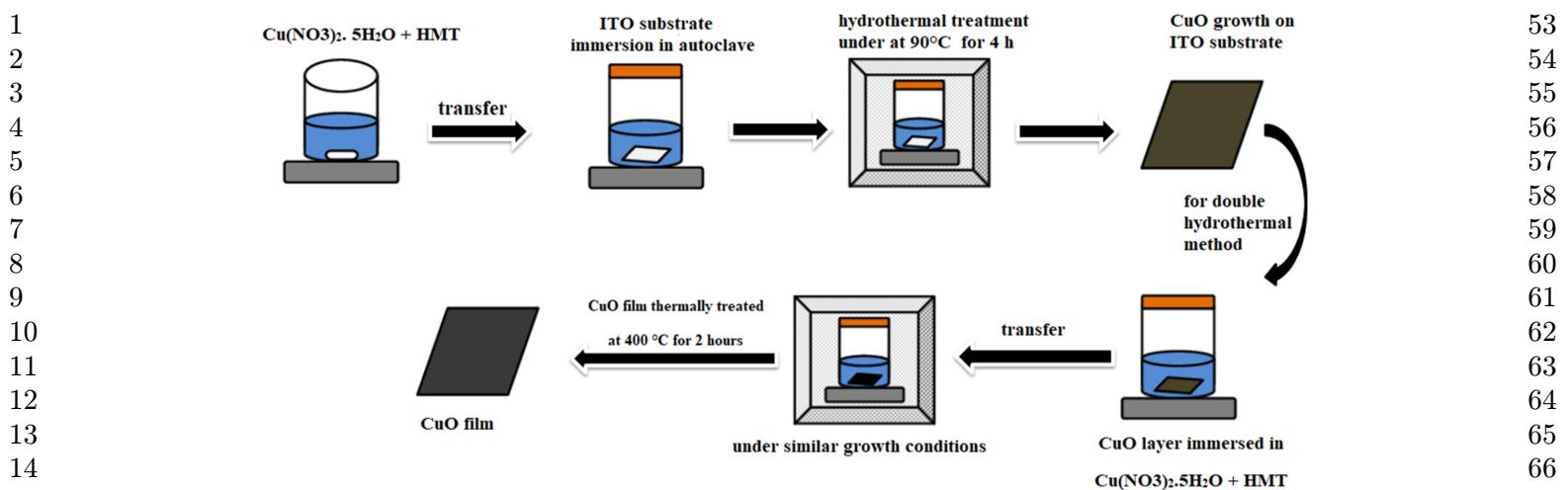


Fig. 1. Scheme of synthesis of CuO NRs using double-hydrothermal setup.

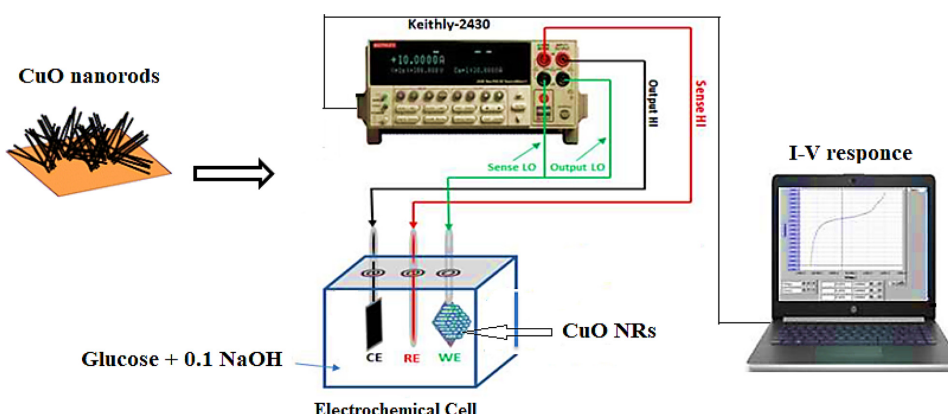


Fig. 2. Schematic illustration of nonenzymatic glucose sensor electrode fabrication and its application in glucose detection.

(a working electrode (WE), a counter electrode (CE), and a reference electrode (RE). The CuO NRs were represented by the working electrode (WE), graphite was used as the counter electrode (CE), and Ag/AgCl was used as the reference electrode (RE). Cyclic voltammetry (CV) was used to characterize electrodes in 0.1 M (NaOH) (supporting electrolyte) with varying concentrations of glucose (0.5, 1 and 2) mM at a scan rate of 200 mVs⁻¹. At +0.1 V, CuO chronoamperometric responses were measured. The electrodes were kept in the air at room temperature. All of the experiments were repeated three times at room temperature to ensure that they were repeatable.

technique at three different concentrations (0.02, 0.04 and 0.06) M. All of the peaks may be attributed to CuO's monoclinic phase (JCPDS 45-0937), and no impurity peaks can be found, showing that the CuO nanostructures are pure and well crystallized. The high resolution of the principal diffraction peaks indicated the CuO NRs' crystallinity, and peak intensity decreased as molar concentration increased. The decrease in the intensity of the XRD peak is mainly attributed to the effects caused in the diffractogram by the micro deformation, coherent domain, and instrumental effects.²⁸

The average crystallite size of strong peaks (preferable orientation) was calculated based on the Debye-Scherrer formula²⁹

$$D = \frac{0.9\lambda}{\beta \cos\theta}, \quad (1)$$

where D is the crystal size, λ is the XRD beam wavelength (1.5408), β is the peak's full-width

3. Results and Discussion

3.1. XRD analyses

Figure 3 shows the XRD patterns of CuO NRs on ITO substrate obtained using the double-hydrothermal

H. A. Jasim & O. A. A. Dakhil

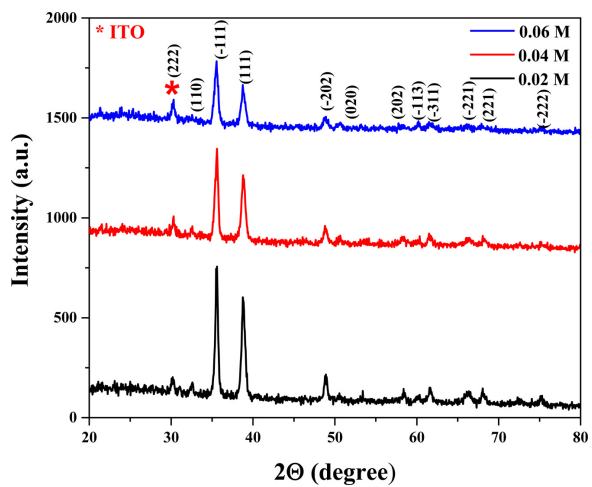


Fig. 3. XRD pattern of CuO as prepared by a double hydrothermal method.

half-maximum in radians, and θ is the Bragg angle. The thick film suffers from microstrain and dislocations as a result of the heat treatment process. The equation³⁰ is used to calculate the dislocation density (δ):

$$\delta = \frac{1}{D^2}. \quad (2)$$

The film's microstrain ε was calculated using the following formula:

$$\varepsilon = \frac{\beta \cos \theta}{4}. \quad (3)$$

Table 1 shows the crystallite size (D), dislocation density (δ), and Micro strain (ε) of CuO NRs calculated from XRD patterns with preferable orientations (-111). The crystallite size of the preferred peak obtained was decreased when molar concentration increased.

3.2. Morphology of CuO NRs (FE-SEM)

Next, morphologies of the as-synthesized CuO NRs were examined by FE-SEM, as shown in Figs. 4(A)–4(C). Obviously, in the images, the CuO NRs aggregate as flower-like structures in Fig. 4(A). On the ITO substrate, CuO was found to be uniformly and vertically grown. Thus, increasing the concentration from 0.02 M to 0.06 M increased the length of CuO nanorods since the number of nuclei increased which further coalesce to decrease the surface energy of the system. In other words, observed that by

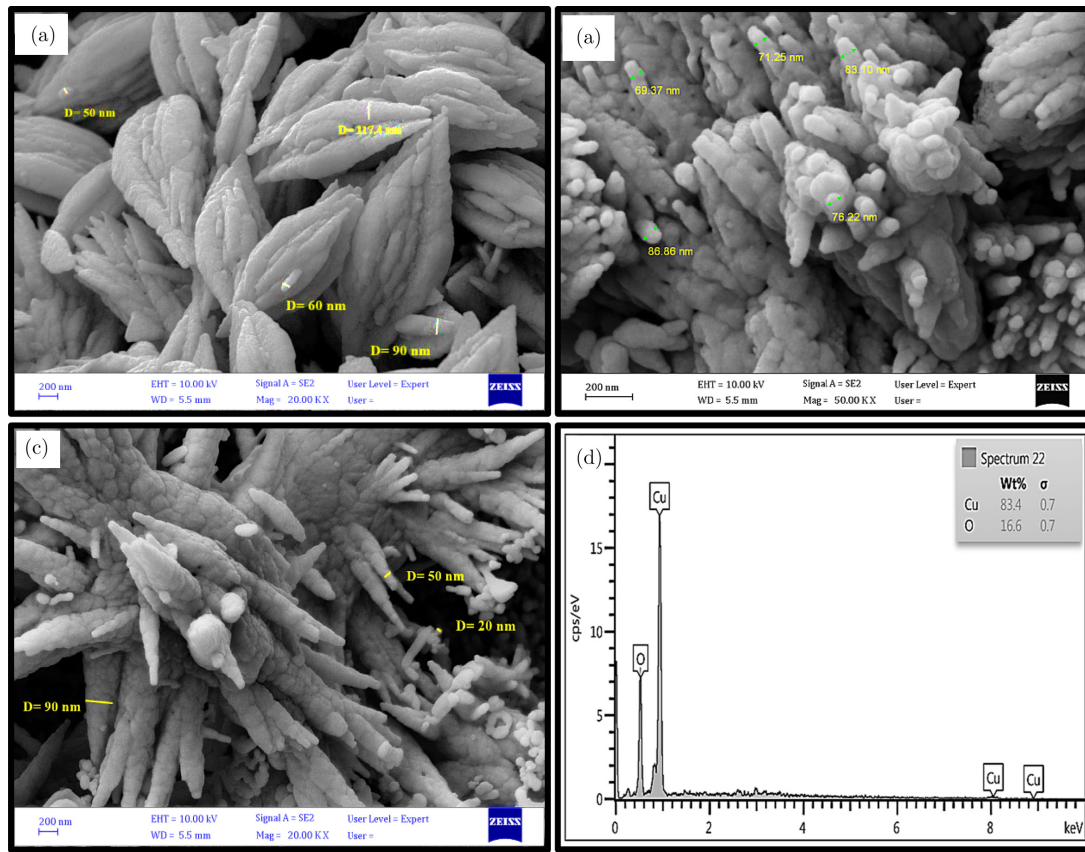


Fig. 4. (A)–(C) FE-SEM surface images of CuO by double-hydrothermal technique, and (D) EDX analysis.

Synthesis of CuO NRs Using a Double Hydrothermal Method

1
2
3
4
5
6
7
8
9
10
11
12
13
14
15
16
17
18
19
20
21
22
23
24
25
26
27
28
29
30
31
32
33
34
35
36
37
38
39
40
41
42
43
44
45
46
47
48
49
50
51
52

Table 1. Structural parameters of CuO NRs by the double-hydrothermal method.

Material	Concentration (M)	D (nm)	δ (10^{10}) cm^{-2}	$\varepsilon \cdot 10^{-3}$
CuO	0.02	23	18.8	1.50
	0.04	17.6	32.07	1.96
	0.06	14.8	45.5	2.33

increasing the concentration from (0.02 M to 0.06 M) of the hydrothermal treatment the particles size of the obtained structure was decreased, this agree with XRD results as-explained in Table 1. Also, as seen in Fig. 4(D), EDX shows in the structure, that there are Cu and O components with different weight percentages are 83.4% and 16.6%, respectively.

3.3. UV–Vis spectra analyses

Figure 5 shows the UV–Visible absorption spectra of CuO NRs structures. The absorption peak of pure CuO NRs is about 350 nm. For three distinct concentrations of CuO NRs, UV–Vis spectroscopy revealed a broad characteristic absorption band near 300 nm. Among the two, CuO NRs prepared at the highest concentration (0.06 M) had the highest absorbance (0.02 and 0.04 M).

The optical transition involved in as-synthesized CuO NRs can be estimated using the Tauc relation,³¹ which is based on the dependence of α on $h\nu$.

$$\alpha = \frac{A(h\nu - E_g)}{h\nu}. \quad (4)$$

The optical energy gap between the bottom of the conduction band and the top of the valance

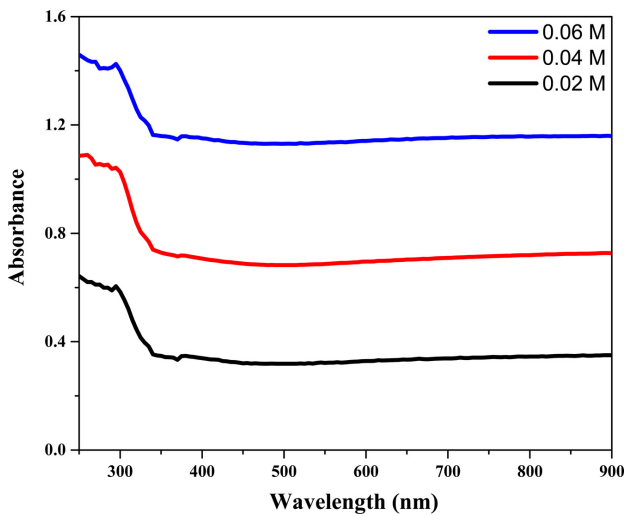
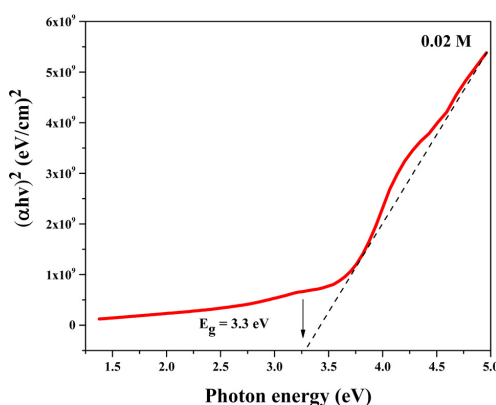


Fig. 5. The absorption spectra of CuO as-prepared by the double-hydrothermal method with different concentrations.

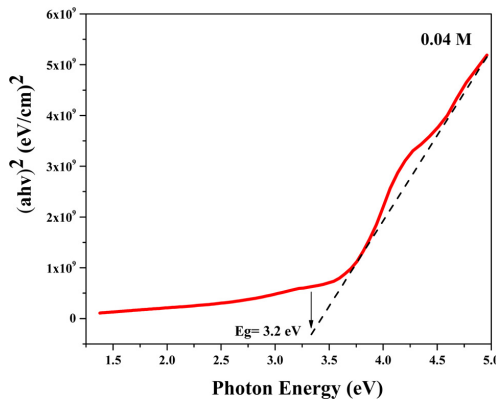
band was supposed to be E_g , B was a constant, and n was the index, which was assumed to be 0.5 for indirect transition and 2 for direct transition. The bandgap of CuO NRs was observed to be synthesized utilizing a double hydrothermal process with varying concentrations (0.02, 0.04 and 0.06). The estimated bandgap was found to be about 3.3, 3.1 and 3 eV, respectively. This referred to an expansion in the energy gap due to the phenomenon of quantum confinement (Fig. 6).

3.4. Free-enzymatic glucose measurements

The electrocatalytic activity of the CuO electrode towards the oxidation of glucose in an alkaline solution was tested in 0.1 M NaOH solution in the presence and absence of glucose, respectively, at a scan rate of 200 mV/s for the fabrication of a nonenzymatic glucose sensor. CuO NRs on ITO substrate with different concentrations were used as the working electrode. The sensor performances of the fabricated sensor were



(a)



(b)

Fig. 6. Energy band gap of CuO NRs as prepared using double hydrothermal method.

H. A. Jasim & O. A. A. Dakhil

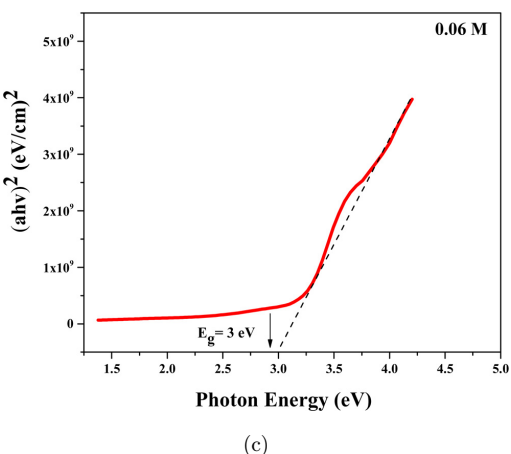


Fig. 6. (Continued)

examined by using the I - V technique. All the measurements were carried out at room temperature. Interestingly, it was observed that the fabricated glucose sensor exhibited a significant enhancement in

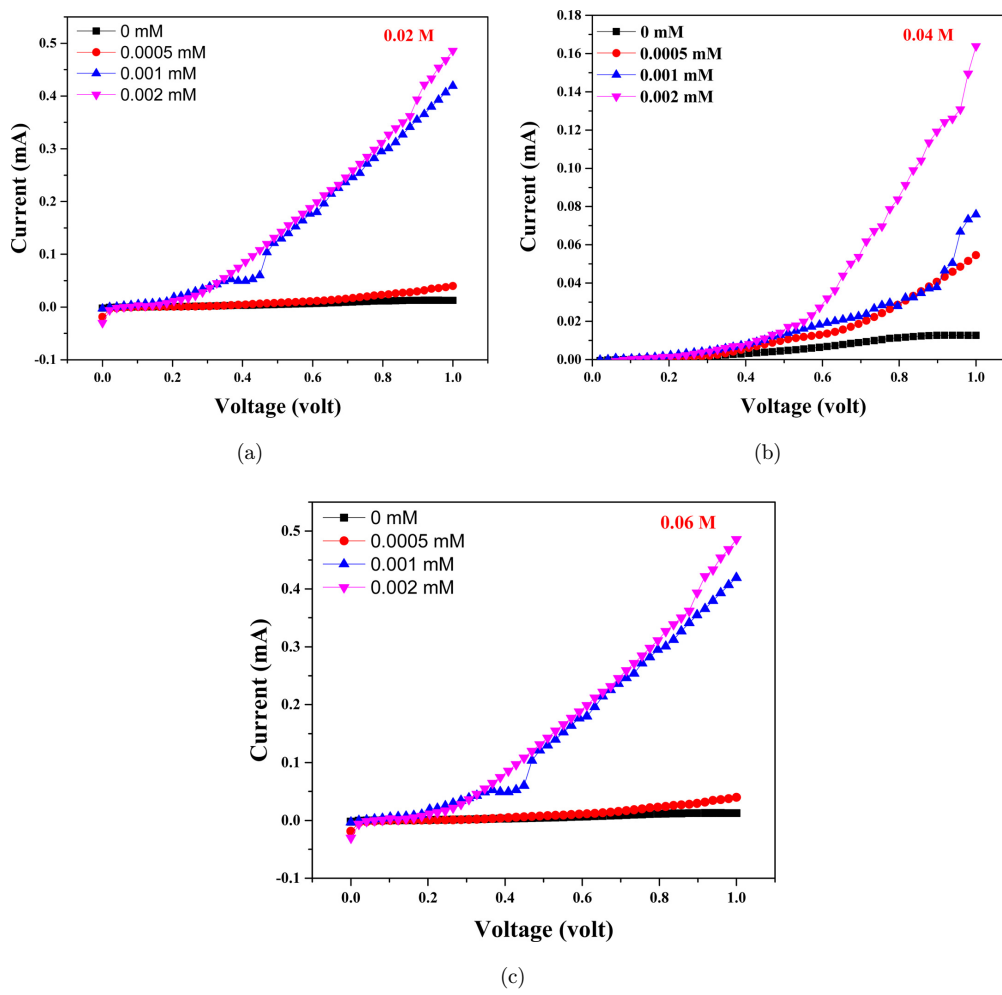


Fig. 7. I - V characteristics of CuO prepared using the double hydrothermal method, (A) 0.02 M, (B) 0.04 M and (C) 0.06 M.

the current with applied voltage (0–1) volt upon the addition of (0.5, 1 and 2) mM of glucose.

In the absence of glucose, only a small background current and no peaks are observed, however when CuO NRs electrode is utilized with (0.5, 1 and 2) mM of glucose, a substantial rise in current signal with a wave potential of roughly +0.5 V is observed. CuO NRs have significantly improved the electrode's performance and electrocatalytic capacity toward glucose oxidation, which may be due to their large surface area, high surface energy, and higher electron transfer ability.³²

In comparison to pure 0.02 M and 0.04 M, a maximum current response of 0.5 mA is attained in 0.06 M as shown in Fig. 7(C). Furthermore, because the response is linear, the conductivity may be calculated using the linear relationship's slope. A short-circuit between the granular nanostructure forms during temporal relaxation, resulting in the rapid increase in total current throughout the sensor, which explains the sensor's regular behavior.

AQ: in Fig. 7 first part label "C" has been changed into "A". Please check and confirm

Ok, thanks for the correction

Synthesis of CuO NRs Using a Double Hydrothermal Method

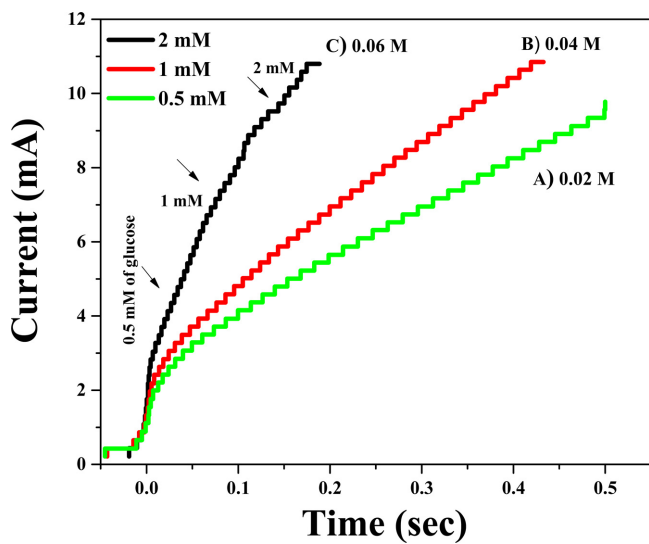


Fig. 8. $I-t$ curves of CuO NRs by double hydrothermal method with an increasing glucose concentration.

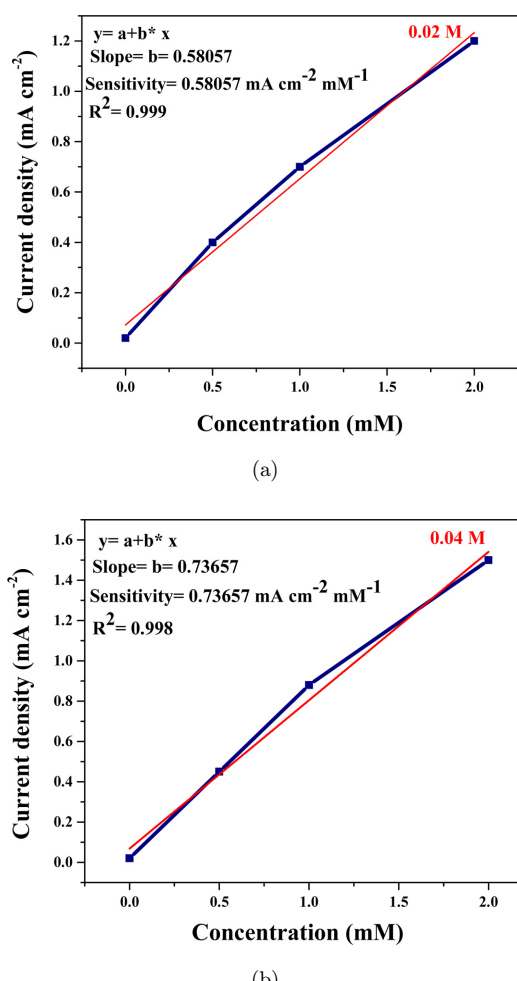


Fig. 9. Sensitivity and a calibration curve of CuO using the double hydrothermal method, (A) 0.02 M, (B) 0.04 M and (C) 0.06 M.

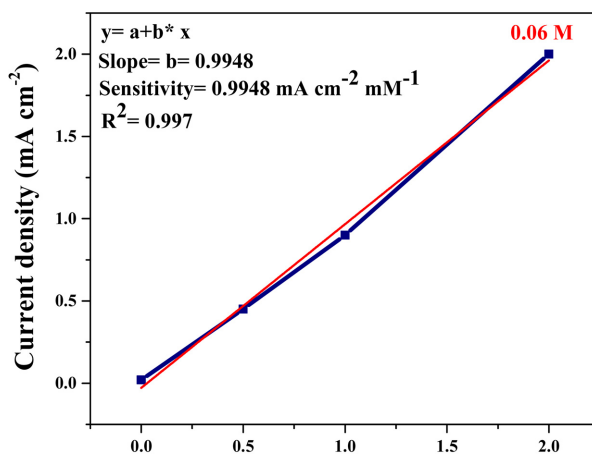


Fig. 9. (Continued)

Table 2. Comparison of various free-enzymatic electrochemical sensors based on CuO electrodes.

Electrode	Sensitivity $\mu\text{A cm}^{-2} \text{ Mm}^{-1}$	Linear Range (mM)	Lower limit of Detection (LOD) μM	Refs.
CuO/GCE nanofibers	431.3	0.006–2.5	0.8	33
Mesoporous CuO	26.6	0.1–3	1.7	34
CuO/graphene	37.63	5–14	0.21	35
CuO nanorods	371.43	4–8	4	26
CuO NRs	580, 736 and 994	0.5–2	0.44, 0.4 and 0.35	This work

For the majority of the glucose concentrations studied, the reaction increases as the test time duration increases at an interval of 50 s, as seen in Fig. 8, this results also agree with the reference was reported in Ref. 26.

Figure 9 shows the sensitivity of CuO NRs prepared by double hydrothermal with different concentrations (0.02, 0.04 and 0.06) for glucose detection without the usage of enzymes. According to the correlation coefficient, the current density of the CuO biosensor has a linear connection as a function of glucose content, as shown in Fig. 9. Surprisingly, CuO thin films as prepared by this method significantly boost sensitivity at low glucose concentrations (Table 2).

4. Conclusions

Highly sensitive CuO NRs bio-sensors were successfully synthesized using a new simple process

53
54
55
56
57
58
59
60
61
62
63
64
65
66
67
68
69
70
71
72
73
74
75
76
77
78
79
80
81
82
83
84
85
86
87
88
89
90
91
92
93
94
95
96
97
98
99
100
101
102
103
104

AQ: Please provide page number for the ref.
167:107504

H. A. Jasim & O. A. A. Dakhil

1 a low-cost, high-benefit (double hydrothermal
 2 method) with different concentrations (0.02, 0.04
 3 and 0.06) M. XRD patterns of CuO explained all of
 4 the peaks may be attributed to CuO's monoclinic
 5 phase. FE-SEM presented nano rod-like shapes with
 6 a diameter range of 20–100 nm and was found to be
 7 uniformly and vertically grown on the ITO substrate.
 8 Besides, CuO NRs prepared at the highest
 9 concentration (0.06 M) had the highest absorbance
 10 with energy gap. Compared with variations in
 11 concentrations, the CuO sensor achieved excellent
 12 glucose sensitivity in a linear range (0.5–2 mM) of
 13 glucose, especially at 0.06 M with energy band gap
 14 about 3 eV. As a result, as the data reveal, the
 15 morphology of CuO NRs generated using this pro-
 16 cess is critical in confirming the electrode's efficiency
 17 for glucose sensing without the usage of mediators.
 18 It has a very high sensitivity of (5805.7, 7365.7
 19 and 994.8) $\mu\text{A Mm}^{-1} \text{cm}^{-2}$ with LOD (0.44, 0.4 and
 20 0.35) μA , a higher linear range of up to 2 mM, and
 21 robust stability when compared to the other elec-
 22 trodes. Based on electrochemical tests, CuO NRs
 23 electrodes offer a lot of potential for use as a non-
 24 invasive nonenzymatic glucose biosensor. Based on
 25 these promising results, CuO is a potential nano-
 26 material for future design and microfabrication
 27 of bioelectrochemical nanodevices for glucose
 28 detection.

Acknowledgments

The authors are grateful to the Department of Physics, College of Science, Mustansiriyah University, Baghdad, Iraq (<https://uomustansiriyah.edu.iq>) for their support and assistance. Also, we want to express our gratitude to the Lab personnel for their support and efforts.

References

1. Y. Marunaka, *World J. Diabet.* **6**, 125 (2015).
2. C. P. Domingueti, L. M. S. A. Dusse, M. das Graças Carvalho, L. P. de Sousa, K. B. Gomes and A. P. Fernandes, *J. Diabetes Complicat.* **30**, 738 (2016).
3. M. A. Akhtar, R. Batool, A. Hayat, D. Han, S. Riaz, S. U. Khan, M. Nasir, M. H. Nawaz and L. Niu, *ACS Appl. Nano Mater.* **2**, 1589 (2019).
4. R. Ahmad, M. Vaseem, N. Tripathy and Y.-B. Hahn, *Anal. Chem.* **85**, 10448 (2013).
5. V. E. Coyle, A. E. Kandjani, M. R. Field, P. Hartley, M. Chen, Y. M. Sabri and S. K. Bhargava, *Biosens. Bioelectron.* **141**, 111479 (2019).
6. J. Xiao, Y. Liu, L. Su, D. Zhao, L. Zhao and X. Zhang, *Anal. Chem.* **91**, 14803 (2019). 53
 54
7. R. Ahmad, M. Khan, M. R. Khan, N. Tripathy, M. I. R. Khan, P. Mishra, M. A. Syed and A. Khosla, *Microsyst. Technol.* **1** (2020). 55
 56
8. W. Han, H. He, L. Zhang, C. Dong, H. Zeng, Y. Dai, L. Xing, Y. Zhang and X. Xue, *ACS Appl. Mater. Interfaces* **9**, 29526 (2017). 57
 58
9. R. Ahmad, M. Khan, N. Tripathy, M. I. R. Khan and A. Khosla, *J. Electrochem. Soc.* **167**, 107504 (2020). 60
 61
10. H. Huo, C. Guo, G. Li, X. Han and C. Xu, *RSC Adv.* **4**, 20459 (2014). 62
 63
11. S. Liu, B. Yu and T. Zhang, *Electrochim. Acta* **102**, 104 (2013). 64
 65
12. F. Foroughi, M. Rahsepar, M. J. Hadianfard and H. Kim, *Microchim. Acta* **185**, 57 (2018). 66
 67
13. C. Espro, N. Donato, S. Galvagno, D. Aloisio, S. G. Leonardi and G. Neri, *Chem. Eng. Trans.* **41**, 415 (2014). 68
 69
14. P. Chakraborty, S. Dhar, K. Debnath and S. P. Mondal, *J. Electroanal. Chem.* **833**, 21 (2019). 70
 71
15. Z. Liu, B. Yadian, H. Liu, C. Liu, B. Zhang, R. V. Ramanujan and Y. Huang, *Electrochim. Commun.* **33**, 138 (2013). 72
 73
16. J. Wang, *Chem. Rev.* **108**, 814 (2008). 74
 75
17. P. Si, P. Chen and D.-H. Kim, *J. Phys. Chem. B* **1**, 2696 (2013). 76
 77
18. S. Liu, J. Tian, L. Wang, Y. Luo, W. Lu and X. Sun, *Biosens. Bioelectron.* **26**, 4491 (2011). 78
 79
19. S. Guo, D. Wen, Y. Zhai, S. Dong and E. Wang, *ACS Nano* **4**, 3959 (2010). 80
 81
20. Y. Li, Y. Song, C. Yang and X.-H. Xia, *Electrochim. Commun.* **9**, 981 (2007). 82
 83
21. K. E. Toghill and R. G. Compton, *Int. J. Electrochem. Sci.* **5**, 1246 (2010). 84
 85
22. L. Xu, Q. Yang, X. Liu, J. Liu and X. Sun, *RSC Adv.* **4**, 1449 (2014). 86
 87
23. Y. Ding, Y. Wang, L. Su, M. Bellagamba, H. Zhang and Y. Lei, *Biosens. Bioelectron.* **26**, 542 (2010). 88
 89
24. P. Si, X.-C. Dong, P. Chen and D.-H. Kim, *J. Phys. Chem. B* **1**, 110 (2013). 90
 91
25. S. Liu, J. Tian, L. Wang, X. Qin, Y. Zhang, Y. Luo, A. M. Asiri, A. O. Al-Youbi and X. Sun, *Catal. Sci. Technol.* **2**, 813 (2012). 92
 93
26. X. Wang, C. Hu, H. Liu, G. Du, X. He and Y. Xi, *Sens. Actuat. B* **144**, 220 (2010). 94
 95
27. L. Zhang, H. Li, Y. Ni, J. Li, K. Liao and G. Zhao, *Electrochim. Commun.* **11**, 812 (2009). 96
 97
28. D. P. Volanti, D. Keyson, L. S. Cavalcante, A. J. Simoes, M. R. Joya, E. Longo, J. A. Varela, P. S. Pizani and A. G. Souza, *J. Alloys Comp.* **459**, 537 (2008). 98
 99
29. R. Saadon and O. A. Azeez, *Energy Proc.* **50**, 445 (2014). 100
 101
30. R. S. Sabry and O. AbdulAzeez, *Manuf. Lett.* **2**, 69 (2014). 102
 103

Synthesis of CuO NRs Using a Double Hydrothermal Method

1	31. E. Reitz, W. Z. Jia, M. Gentile, Y. Wang and Y. Lei, <i>Electroanalysis</i> 20 , 2482 (2008).	53
2	32. C.-E. Cheng, S. Tangsuwanjinda, H.-M. Cheng and P.-H. Lee, <i>Coatings</i> 11 , 936 (2021).	54
3		55
4		56
5		57
6		58
7		59
8		60
9		61
10		62
11		63
12		64
13		65
14		66
15		67
16		68
17		69
18		70
19		71
20		72
21		73
22		74
23		75
24		76
25		77
26		78
27		79
28		80
29		81
30		82
31		83
32		84
33		85
34		86
35		87
36		88
37		89
38		90
39		91
40		92
41		93
42		94
43		95
44		96
45		97
46		98
47		99
48		100
49		101
50		102
51		103
52		104